

Contents lists available at ScienceDirect

Computers and Mathematics with Applications



www.elsevier.com/locate/camwa

A constrained variational model of biomolecular solvation and its numerical implementation



Yuanzhen Shao a, Elizabeth Hawkins b, Kai Wang c, Zhan Chen b,*

- ^a Department of Mathematics, University of Alabama, Tuscaloosa, AL, United States of America
- b Department of Mathematical Sciences, Georgia Southern University, Statesboro, GA, United States of America
- ^c Department of Computer Science, Georgia Southern University, Statesboro, GA, United States of America

ARTICLE INFO

ABSTRACT

Keywords: Biomolecular solvation Poisson-Boltzmann Variational PDE method Global minimizer Variational based solvation models of biomolecules with smooth interface have drawn attentions in the past decade since they have been developed as an efficient and reliable representation of solute-solvent interfaces in the framework of implicit solvent models. This work aims at providing solid mathematical supports for a promising geometric flow based computational solvation model with smooth interface (GFBSS) and its involved computational treatments. For this purpose, we improve the GFBSS model by explicitly including two physical constraints: (1) a novel experimental based domain decomposition, and (2) a two-sided obstacle for the characteristic function describing the optimal diffuse solute-solvent boundary. It is shown that the resulting constrained model is mathematically well-posed. Further, to overcome the challenges arising from including these constraints, we propose a family of generalized constrained energy functionals whose variations satisfy a *q*-Laplacian type equation for nonpolar molecules. The solvation free energies predicted by the generalized models converge to that of the proposed constrained one. Most importantly, the numerical difference between the generalized models and the previous unconstrained GFBSS model is negligible. It implies that the newly proposed constrained solvation model and the previous unconstrained one are equivalent to each other in terms of the solvation free energy calculation and prediction. Our model validation, its numerical implementation, and solvation energy convergence have been demonstrated using several common biomolecular modeling tasks.

Contents

1.				
	1.1.	List of no	tations	19
2.	Mather	natical mo	del and its analysis	19
	2.1.	The total	energy functional	19
	2.2.	The gene	ralized Poisson-Boltzmann equation	20
	2.3.	Minimizi	ng the total energy functional	21
	2.4.	Asympto	tic behavior of $I_a(\cdot)$ as $q o 1^+$	21
	2.5.	Variation	s and surface models	23
3.	Compu	itational sc	hemes and simulation results	24
	3.1.	Numerica	ıl implementation	24
	3.2.	Simulatio	on results	25
		3.2.1.	Model validation	25
		3.2.2.	Minimized energy converges when $q \rightarrow 1^+$	25
		3.2.3.	Comparison with previous GFBSS	26
4.				
Ackno	wledgen	nents		27
Refere	nces			27

E-mail address: zchen@georgiasouthern.edu (Z. Chen).

https://doi.org/10.1016/j.camwa.2021.12.009

Received 28 June 2021; Received in revised form 29 November 2021; Accepted 18 December 2021

k Corresponding author.

1. Introduction

Solute-solvent interactions are typically described by solvation energies (or closely related quantities): the free energy of transferring the solute from a vacuum to the solvent environment of interest (e.g., water at a certain ionic strength). Solvation free energies can be calculated by a variety of computational methods ranging from very time-consuming quantum mechanical approaches to simple phenomenological modifications of Coulomb's law. Implicit solvent methods have become popular for many applications in molecular simulation [2,5,20]. A variety of implicit solvent models [2,14,27,40,42,46] are available to describe polar solvation; currently one of the most widely-used methods is the Poisson-Boltzmann (PB) [2,21,24,29]. The separation of the discrete and the continuum domains in implicit solvent models requires an interface to indicate the separation of solute atoms from the surrounding solvent. Many solvation quantities, including surface areas, cavitation volumes, and electrostatic free energies, are sensitive to the interface definition. There are a number of different surface definitions, which include the van der Waals (vdW) surface, the solvent excluded surface (SES) and the solvent accessible surface (SAS), available for implicit solvent applications. These surface models do have much success in biomolecular modeling tasks such as protein folding, protein-protein interactions, and macromolecular docking. However, they are ad hoc partitions and may create geometric singularities. In addition, it has been observed that these surface definitions either non-negligibly overestimate or underestimate the solvation free energies [44].

In the framework of PB based implicit solvent approach, variational models of solvation have recently received attention [7,17,45,47,48, 50]. Among them, geometric flow based solvation model with smooth interface (GFBSS) [7] stands out as one of pioneering work. It not only incorporates descriptions of solvent-solute interactions and polarnonpolar coupling but also generates optimal diffuse interface between solute and solvent by the minimization of proposed energy functional. In particular, it aims at a physically realistic smooth solvent-solute boundary. The usage of smooth interface (related to inhomogeneous dielectric profile) can be justified physically and biologically. First of all, there should be a smooth transition region, in which atoms of solute and solvent are mixed, between the SES surface and SAS surface. From a quantum mechanical point of view, biomolecules interact with solvent molecules and/or other biomolecules, and their wave functions and their electron density distributions overlap spatially. In addition, when considering the structures of water and ions around the biomolecules or close to the charged surface in PB equations, an effective positiondependent dielectric function is needed to describe the smoothly varying dielectric property in the solvent domain [1,4,28].

The main idea of GFBSS model is to introduce a characteristic function u to describe the distribution of solute throughout the domain (u=1 for pure solute and u=0 for pure solvent) [7]. Then the minimization of a proposed total energy functional leads to an optimal profile of the characteristic function, which is defined as the smooth solvent-solute boundary between the atomic solute domain and continuum solvent domain. Specifically, the following total solvation free energy was proposed in terms of u:

$$I = \int_{\Omega} \gamma |\nabla u(\mathbf{r})| d\mathbf{r} + \int_{\Omega} P_h u(\mathbf{r}) d\mathbf{r} + \int_{\Omega} \rho_s (1 - u(\mathbf{r})) U^{\text{vdW}}(\mathbf{r}) d\mathbf{r}$$

$$+ \int_{\Omega} \left\{ u \left[\rho_m(\mathbf{r}) \psi(\mathbf{r}) - \frac{1}{2} \epsilon_m |\nabla \psi(\mathbf{r})|^2 \right] \right.$$

$$+ (1 - u) \left[-\frac{1}{2} \epsilon_s |\nabla \psi(\mathbf{r})|^2 - \beta^{-1} \sum_{j=1}^{N_c} c_j^{\infty} (e^{-\beta q_j \psi(\mathbf{r})} - 1) \right] \right\} d\mathbf{r}, \tag{1}$$

Here $\int_{\Omega} \gamma |\nabla u(\mathbf{r})| d\mathbf{r}$ is used to describe the surface energy of the macromolecule. It measures the disruption of intermolecular and/or intramolecular bonds that occurs when a surface is created. $\int_{\Omega} P_h u d\mathbf{r}$ is the mechanical work of creating the biomolecular size vacuum in the solvent. ρ_s is the solvent bulk density, and $U^{\text{vdW}}(\mathbf{r})$ is the attractive portion of the van der Waals potential at point \mathbf{r} . It represents the attractive dispersion effects near the solvent-solute interface and has been shown by Wagoner and Baker [44] to play a crucial role in accurate nonpolar solvation analysis. In the second and third lines of (1), ψ is the electrostatic potential; ρ_m is the density of molecular charges; ϵ_m and ϵ_s are the dielectric constants of the molecule and the solvent, respectively. Usually, $\epsilon_m \approx 1$ for the protein and $\epsilon_s \approx 80$ for the water. q_j is the charge of ion species $j=1,2,\cdots,N_c$; k_B is the Boltzmann constant; T is the absolute temperature; c_j^∞ is the bulk concentration of the j-th ionic species; and $\beta=1/k_BT$. For notational brevity throughout this paper, we put

$$B(s) = \beta^{-1} \left[\sum_{j=1}^{N_c} c_j^{\infty} \left(e^{-\beta s q_j} - 1 \right) \right].$$

The first three terms of (1) are usually termed the nonpolar portion of the solvation energy. The remaining terms are called the polar portion of the solvation energy.

With improved parameterization and solution schemes, GFBSS models have been developed as an efficient and reliable representation of solute-solvent interfaces by accounting for varying dielectric constants near the molecules in a natural means [7,13,43,45,49]. In spite of its success in solvation prediction and model applications, there are several mathematical questions that need to be pursued and investigated for its further model development, analysis and applications. One is about the existence of a non-trivial physically meaningful global minimizer of the proposed energy functional. For instance, regarding nonpolar molecules, one only needs to consider the first three terms of equation (1). Consequently, u = 0 throughout the domain may become a trivial global minimizer. That leads to zero or negative nonpolar free energy which is supposed to be positive based on biological measurement. To avoid this type of nonphysical outcome, a biological fact has been taken into consideration in previous numerical implementations (the first numerical constraint): there is no solute atom outside a boundary (such as SAS surface) and there should exist continuous pure solute region without solvent atoms inside it. As a result, u was fixed to be 1 for the pure solute region and 0 in the pure solvent area. Then the targeted optimal u profile is only to be determined in the transition area [7] between the pure solute and the pure solvent regions.

The second theoretical consideration of the previous GFBSS model stems from the following question: how can one assure that the global minimizer $0 \le u^* \le 1$ as designed for a solute density function? Numerically, a simple cut-off strategy together with relaxing schemes has been applied to the solution process to guarantee $u \in [0,1]$ [7] (the second numerical constraint): u is set to be zero when a computed value is below zero and 1 when it is above 1.

This work aims at providing rigorous theoretical supports for the previous unconstrained GFBSS model [7] and its associated numerical strategies. To the end, we improve the previous unconstrained GFBSS model by explicitly incorporating the two aforementioned numerical constraints: (1) a novel experimental based domain decomposition, and (2) a two-sided obstacle for the characteristic function describing the optimal diffuse solute-solvent boundary. The proposed constrained model is proved to be mathematically well-posed.

However, including the two numerical constraints in equation (1) generates an essential difficulty in determining its first variation. This makes the numerical computations of the solvation energy, i.e. the minimum energy predicted by equation (1), a challenging task. To overcome

this difficulty, we further propose a family of q-energy type functionals with the same constraints. It is proved that their minimum energies and minimizers converge to those of equation (1) with constraints. Such constrained q-energy functionals are known to lead to variational inequalities. For nonpolar molecules, we are able to transform these inequalities into q-Laplacian type equations. Based on these analyses, numerical implementation and validation of the generalized solvation models are given as well as its numerical comparison with the previous GFBSS model.

The rest of this paper is organized as follows. We first describe in details our new constrained total solvation energy functional and the corresponding q-energy type functionals in Section 2.1. Then the existence and uniqueness of global minimizers of these functionals are studied in Section 2.2 and 2.3. The convergence of the energies predicted by the constrained q-energy functionals is proved in Section 2.4. It is followed by a variational process to derive the interface models for surface generation in Section 2.5. Finally, numerical validation and complementary simulation of constrained variational model are demonstrated in Section 3. Section 4 is the concluding remark.

1.1. List of notations

In this article, we use $\mathbf{r} = (x, y, z)$ to denote the coordinates in \mathbb{R}^3 . Given two vectors $u, v \in \mathbb{R}^3$, $u \cdot v$ is their inner product. \mathcal{L}^3 and \mathcal{H}^2 always stand for the Lebesgue measure in \mathbb{R}^3 and the 2-dimensional Hausdorff measure, respectively.

Given $U \subseteq \mathbb{R}^3$, \overline{U} stands for the closure of U. The topological boundary of U is denoted by ∂U .

Suppose that X is a Banach space. Given a sequence $\{u_k\}_{k=1}^{\infty} = (u_1, u_2, \cdots)$ in X, $u_k \to u$ in X means that u_k converge weakly to some $u \in X$

Given $1 \leq p < \infty$, $L^p(U)$ denotes the set of all p-integrable (Lebesgue) measurable functions defined on $U \subset \mathbb{R}^3$; and when $p = \infty$, $L^p(U)$ stands for the space of all essentially bounded measurable functions. We denote their norms by $\|\cdot\|_p$. $W^{k,p}(U)$ is the Sobolev space consisting of functions whose weak derivatives up to k-th power belong to $L^p(U)$; $H^1(U) = W^{1,2}(U)$; BV(U) consists of all functions $f \in L^1(\Omega)$ that are of bounded variation in U, whose total variation in U is denoted by $\|Df\|(U)$. Their norms are denoted by $\|\cdot\|_{W^{1,q}}$, $\|\cdot\|_{H^1}$ and $\|\cdot\|_{BV}$, respectively. $W_0^{k,p}(U)$ and $H_0^1(U)$ mean the closure of $C_0^\infty(U)$ in $W^{k,p}(U)$ and $H^1(U)$, respectively.

2. Mathematical model and its analysis

2.1. The total energy functional

Experimentally, it has been known that beyond a boundary (such as solvent excluded surface), which encloses the immersed molecules, solvent atoms are not present. Moreover, as described in the introduction, the wave functions of the solute and solvent overlap spatially as well as their electron density distributions. Therefore, there must be a mixing region of the solvent and solute. Based on these considerations, we explicitly introduce a novel domain decomposition for the whole computational domain as follows.

Let $\Omega \subseteq \mathbb{R}^3$ be a bounded and connected Lipschitz domain composed of three disjoint subdomains with Lipschitz boundaries:

- Ω_m : solute (molecular) region;
- Ω_s : solvent region;
- Ω_b: solute-solvent mixing region.

All three subdomains are predefined. We further assume that $\partial\Omega\subset\partial\Omega_s$ and $\partial\Omega_m\subset\partial\Omega_b$. Let

$$\Sigma_1 = \partial \Omega_m$$

be the solvent excluded surface enclosing the pure solute region and

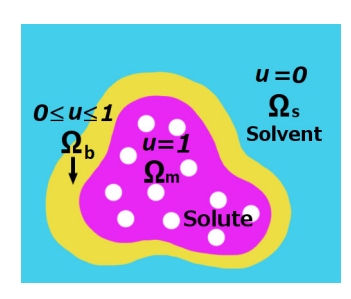


Fig. 1. Illustration of model domain definition and decomposition: $Ω_m$: solute (molecular) region; $Ω_s$: solvent region; $Ω_s$: solute-solvent mixing region.

$$\Sigma_{\Omega} = \partial \Omega_{\alpha} \setminus \partial \Omega$$
,

be the solvent accessible surface outside of which is the pure solvent domain. Suppose that $\Sigma_1 \cap \Sigma_0 = \emptyset$ and Ω_m, Ω_s are non-empty. A picture illustration of the domain definition and decomposition can be found in Fig. 1. We further assume that the solute region Ω_m contains N_m solute atoms located at $\mathbf{r}_1, \cdots, \mathbf{r}_N$; and there are N_c ion species outside Ω_m .

Moreover, we revise the previous definition of u and the energy functional based on the domain decomposition shown in Fig. 1. We define $u: \Omega \to \mathbb{R}$ in such a way that $u(\mathbf{r})$ represents the solute volume ratio at position $\mathbf{r} \in \Omega$. As such, the physical constraints

$$u(\mathbf{r}) \in [0,1]$$
 for a.a. $\mathbf{r} \in \Omega$ (2)

and

$$u = 1$$
 a.e. in Ω_m and $u = 0$ a.e. in Ω_s (3)

need to be imposed. Constrain (2) makes the potential minimizer u of the solvation energy functional meaningful as a volume ratio function; Constrain (3), together with the domain decomposition, guarantees that Ω_m and Ω_s are purely occupied by the molecule and the aquatic solvent, respectively. These two conditions ensure that the potential minimizer u is physical.

Furthermore, to overcome the challenges arising from incorporating Constraints (2) and (3) as mentioned in the introduction, we extend the definition of the nonpolar portion of solvation free energy by considering

$$I_{np,q}(u) = \int_{\Omega} \left[\gamma |\nabla u(\mathbf{r})|^q + P_h u(\mathbf{r}) + \rho_s (1 - u(\mathbf{r})) U^{\text{vdW}}(\mathbf{r}) \right] d\mathbf{r}$$

with $q \in [1,2]$. Note that we generalize the surface energy term by extending specific q=1 to the general case $1 \le q \le 2$. When q=1, the term $\int_{\Omega} |\nabla u| \, d\mathbf{r} = \|Du\|(\Omega)$ stands for the total variation of u in Ω , which is adopted in the original formulation in [7]. Note that $U^{\mathrm{vdW}}(\mathbf{r})$ can be formulated by $\sum_i U_i^{\mathrm{att}}(\mathbf{r})$ in which $U_i^{\mathrm{att}}(\mathbf{r})$ represents the attractive part of Lennard-Jones potential [7,44]. To this end, the L-J potential can be divided into attractive U_i^{att} and repulsive U_i^{rep} in different ways. Here we take a Weeks-Chandler-Andersen (WCA) decomposition based on the original WCA theory [31]:

$$\begin{split} U_i^{\mathrm{att,WCA}}(\mathbf{r}) &= \left\{ \begin{array}{ll} -\epsilon_{is}(\mathbf{r}) & 0 < \|\mathbf{r} - \mathbf{r}_i\| < 2^{1/6}\sigma_{is} \\ U_i^{\mathrm{LJ}}(\mathbf{r}) & \|\mathbf{r} - \mathbf{r}_i\| \ge 2^{1/6}\sigma_{is}, \end{array} \right. \\ U_i^{\mathrm{rep,WCA}}(\mathbf{r}) &= \left\{ \begin{array}{ll} U_i^{\mathrm{LJ}}(\mathbf{r}) + \epsilon_{is}(\mathbf{r}) & 0 < \|\mathbf{r} - \mathbf{r}_i\| < 2^{1/6}\sigma_{is} \\ 0 & \|\mathbf{r} - \mathbf{r}_i\| \ge 2^{1/6}\sigma_{is}, \end{array} \right. \end{split}$$

where

$$U_i^{\text{LJ}}(r) = 4\epsilon_{is} \left[\left(\frac{\sigma_{is}}{r} \right)^{12} - \left(\frac{\sigma_{is}}{r} \right)^6 \right]$$

with σ_{is} of length and well depth parameters ϵ_{is} of energy depending on the atom type.

Similarly, the PB theory based polar energy can be defined as

$$I_p(u,\psi) = \int\limits_{\Omega} \left[\rho_m \psi - \frac{1}{2} \epsilon(u) |\nabla \psi|^2 - (1-u) B(\psi) \right] d\mathbf{r},$$

where $\epsilon(u)=u\epsilon_m+(1-u)\epsilon_s$ is the dielectric constant. In addition, we assume the neutral condition

$$\sum_{i=1}^{N_c} c_j^{\infty} q_j = 0.$$
(4)

Physically, u and thus the profile of the solvent-solute boundary, must be determined by the energy minimization principle. Therefore, our task is to identify the energy functional to be optimized, and to evaluate the desired solvent-solute properties depending on u.

With all these preparations, we are now in a position to state the minimization problem of the total energy functional

$$K_a(u,\psi) = I_{np,a}(u) + I_p(u,\psi). \tag{5}$$

In (5), ψ satisfies the boundary value problem of the generalized Poisson-Boltzmann equation (GPBE)

$$\begin{cases} \operatorname{div}(\varepsilon(u)\nabla\psi) + (1-u)B'(\psi) = -\rho_m & \text{in} & \Omega; \\ \psi = \psi_{\infty} & \text{on} & \partial\Omega, \end{cases}$$
 (6)

where $\psi_{\infty} \in W^{1,\infty}(\Omega)$ is a predefined boundary value. Therefore given a measurable u satisfying (2) and (3), $\psi = \psi(u)$ is determined via (6).

Based on (6), the minimization problem (5) can be stated as to minimize

$$I_{q}(u) = \int_{\Omega} \left[\gamma |\nabla u|^{q} + P_{h}u + \rho_{s}(1 - u)U^{\text{vdW}} \right] d\mathbf{r}$$

$$+ \int_{\Omega} \left[\rho_{m}\psi - \frac{1}{2}\epsilon(u)|\nabla\psi|^{2} - (1 - u)B(\psi) \right] d\mathbf{r}, \tag{7}$$

in the admissible space

 $\mathcal{X}_q = \{ u \in W^{1,q}(\Omega) : u \text{ satisfies Constraints (2) and (3)} \},$

when q > 1, and

 $\mathcal{X}_1 = \{ u \in BV(\Omega) : u \text{ satisfies Constraints (2) and (3)} \},$

when q = 1; ψ is determined via (6) in the space

$$\mathcal{A} = \{ v \in H^1(\Omega) : v|_{\partial \Omega} = \psi_{\infty} \}.$$

A couple of comments on the energy functional (7) for the case $q \in (1,2]$ are as follows.

Remarks 2.1.

- (i) In the case $1 < q \le 2$, the functional (7) is strictly convex in u. Based on this fact, we will show in Theorem 2.4 that the minimizer of (7) is unique in \mathcal{X}_a .
- (ii) It is known that a constrain like (2) generates a two-sided obstacle problem, whose variation results in an variational inequality. In the case of $q \in (1,2]$, the knowledge of the porosity of free boundaries of q-Laplacian equations can be adopted to transform the variational inequality into a PDE. Such knowledge, however, is unknown in the case q = 1.

Note that the first variation of $\int_{\Omega} |\nabla u|^q \, d\mathbf{r}$, as will be shown in Section 2.5, produces a term of the form $\Delta_q u := \operatorname{div}(|\nabla u|^{q-2} \nabla u)$. This is called the q-Laplacian operator, which is also termed the p-Laplacian operator in lots of literature. In our manuscript, we adopt the letter "q" instead of "p" to distinguish the notation I_p of the polar energy from the notation of the total energy I_q in (7). The subscript q in the latter is to indicate its dependence on q.

(iii) It is also known that the minimizer of a total variation model, which corresponds to the case q=1, with constraints like (3) usually suffers from jump discontinuity along Σ_i . This may lead to additional computational errors.

(iv) Most importantly, in Section 2.4, we will show that, as $q \to 1^+$, the minimizers u_q of $I_q(\cdot)$ and the corresponding solvation energies converge to their counterparts in the case q=1.

We would like to point out that this result does not follow from the standard convergence results of the solutions of q-Laplacian equations $\Delta_q u = f$ to that of the 1-Laplacian equation. Indeed, such convergence only holds when f satisfies some restrictive conditions in certain function spaces. See [11,15,26,34–36] for some related work.

2.2. The generalized Poisson-Boltzmann equation

Following the ideas in [12,32,33], for any $u \in \mathcal{X}_a$, we set

$$E_u[\psi] = -I_p(u,\psi) = \int\limits_{\Omega} \left[\frac{1}{2} \epsilon(u) |\nabla \psi|^2 - \rho_m \psi + (1-u) B(\psi) \right] \, d\mathbf{r}.$$

Proposition 2.2. Given any $u \in \mathcal{X}_1$, there exists a unique $\psi_u \in \mathcal{A}$ such that

$$E_u[\psi_u] = \min_{w \in \mathcal{A}} E_u[\psi] < \infty.$$

Moreover, ψ_u is the unique weak solution to the boundary value problem (6). Finally, ψ_u satisfies

$$\|\psi_u\|_{H^1} + \|\psi_u\|_{\infty} \le C_0.$$

Particularly, the constant C_0 depends only on ψ_{∞} and can be chosen independent of u.

Proof. (i) First observe that $\epsilon(u) \in L^{\infty}(\Omega)$ with $1 = \epsilon_m \le \epsilon(u) \le \epsilon_s = 80$. By the standard elliptic theory, cf. [23, Theorems 8.3 and 8.16], the boundary value problem

$$\begin{cases} \operatorname{div}(\epsilon(u)\nabla\psi) + \rho_m = 0 & \text{in } \Omega; \\ \psi = \psi_{\infty} & \text{on } \partial\Omega \end{cases}$$

has a unique weak solution $\hat{\psi}_u$, i.e.

$$\int_{\Omega} \epsilon(u) \nabla \hat{\psi}_{u} \cdot \nabla \eta \, d\mathbf{r} = \int_{\Omega} \rho_{m} \eta \, d\mathbf{r}, \quad \forall \eta \in H_{0}^{1}(\Omega),$$
(8)

satisfying

$$\|\hat{\psi}_u\|_{H^1} + \|\hat{\psi}_u\|_{\infty} \le M. \tag{9}$$

The constant M depends only on ψ_{∞} and thus is independent of u.

(ii) Observe that B(0)=0; and (4) implies that B'(0)=0 and $B'(\pm\infty)=\pm\infty$. In addition, B''(s)>0. We thus conclude that $B(0)=\min_{s\in\mathbb{R}}B(s)$ and B is strictly convex. We define $\tilde{E}_u:H^1_0(\Omega)\to\mathbb{R}\cup\{+\infty\}$ by

$$\tilde{E}_{u}[\psi] = \int_{\Omega} \left[\frac{1}{2} \epsilon(u) |\nabla \psi|^{2} + (1 - u) B(\psi + \hat{\psi}_{u}) \right] d\mathbf{r}.$$

By the direct method of calculus of variation, there exists a global minimizer $\bar{\psi}_u \in H^1_0(\Omega)$ of \tilde{E}_u , i.e. $\tilde{E}_u[\bar{\psi}_u] = \min_{\psi \in H^1_0(\Omega)} \tilde{E}_u[\psi]$. Moreover, the strict

convexity of the functional \tilde{E}_u implies that $\bar{\psi}_u$ is the unique global minimizer. Note that by (8)

$$E_{u}[\psi] = \tilde{E}_{u}[\psi - \hat{\psi}_{u}] + \int_{\Omega} \left[\frac{1}{2} \epsilon(u) |\nabla \hat{\psi}_{u}|^{2} - \rho_{m} \hat{\psi}_{u} \right] d\mathbf{r}.$$

Let $\psi_u = \hat{\psi}_u + \bar{\psi}_u$. From the above equality, we learn that

$$E_u[\psi_u] = \min_{w \in A} E_u[\psi].$$

(iii) By the properties of $B(\cdot)$ and (9), there exists some $\lambda > 0$ such that

$$B'(\lambda + \hat{\psi}_u) > 1$$
 and $B'(-\lambda + \hat{\psi}_u) < -1$.

Recall \mathcal{L}^3 is the Lebesgue measure in \mathbb{R}^3 . If $\mathcal{L}^3(\{|\bar{\psi}_u| > \lambda\}) > 0$, we define

$$\tilde{\psi} = \begin{cases} \lambda & \text{on } \{\bar{\psi}_u > \lambda\} \\ \bar{\psi}_u & \text{on } \{-\lambda \leq \bar{\psi}_u \leq \lambda\} \\ -\lambda & \text{on } \{\bar{\psi}_u < -\lambda\}. \end{cases}$$

Then $\tilde{\psi} \in H_0^1(\Omega)$, cf. [16, Proposition 20.2], and $\tilde{E}_u[\tilde{\psi}] \leq \tilde{E}_u[\bar{\psi}_u]$. This contradicts the uniqueness of global minimizer of \tilde{E}_u and thus $|\bar{\psi}_u| \leq \lambda$ a.e.. As a direct consequence, we obtain

$$\|\psi_u\|_{\infty} \le C_1$$

for some C_1 depending only on ψ_{∞} .

(iv) The dominated convergence theorem implies that $\bar{\psi}_u \in H^1_0(\Omega)$

$$\int_{\Omega} \left[\varepsilon(u) \nabla \bar{\psi}_{u} \cdot \nabla \eta + (1 - u) B'(\psi_{u}) \eta \right] d\mathbf{r} = 0$$
(10)

for all $\eta \in H_0^1(\Omega) \cap L^{\infty}(\Omega)$. By a standard approximation argument, it is not hard to see that (10) also holds true for all $\eta \in H_0^1(\Omega)$. Taking $\eta = \bar{\psi}_{\mu}$

$$\int_{\Omega} \left[\varepsilon(u) |\nabla \bar{\psi}_u|^2 + (1 - u) B'(\psi_u) \bar{\psi}_u \right] d\mathbf{r} = 0.$$

Since $|\bar{\psi}_u| \le \lambda$ a.e. and $|B'(\psi_u)| \le C$ for some C depending only on ψ_∞ , we conclude that

$$\|\psi_u\|_{H^1} \le C_2$$
.

Again the constant C_2 depends only on ψ_{∞} . In sum, we can take C_0 = $C_1 + C_2$.

Proposition 2.3. Let $u_k, u \in \mathcal{X}_1$ be such that $u_k \to u$ in $L^1(\Omega)$ as $k \to \infty$. Let $\psi_k, \psi \in A$ be the corresponding electrostatic potentials, i.e.,

$$E_{u_k}[\psi_k] = \min_{w \in A} E_{u_k}[w]$$
 and $E_u[\psi] = \min_{w \in A} E_u[w]$.

Then $\lim_{k \to \infty} E_{u_k}[\psi_k] = E_u[\psi]$.

Proof. The proof is essentially the same as that of [12, Theorem 3.2]. □

2.3. Minimizing the total energy functional

Theorem 2.4. For every $q \in [1,2]$, there exists some $u_q \in \mathcal{X}_q$ such that $I_q(u_q)=\min_{u\in\mathcal{X}_q}I_q(u)$ with $I_q(u_q)$ finite. When $q\in(1,2]$, the minimizer is unique in \mathcal{X}_a .

Proof. The existence of a solution can be proved by using a standard argument in Calculus of Variation. See for example [18, Theorem 8.2.2]. For the reader's convenience, we will present a brief proof. Because several estimates in this proof will be used later in Section 2.4. Given any $u \in \mathcal{X}_a$, recall from Proposition 2.2 that

$$E_u[\psi_u] < E_u[\psi_\infty] \leq \frac{\epsilon_s}{2} \left\| \psi_\infty \right\|_{H^1}^2 + C \left[\left\| \psi_\infty \right\|_\infty + B(\left\| \psi_\infty \right\|_\infty) \right] \leq C_3$$

for some C_3 independent of u and q. Therefore, for any $u \in \mathcal{X}_q$

$$I_{q}(u) = I_{np,q}(u) - E_{u}(\psi_{u}) > I_{np,q}(u) - E_{u}(\psi_{\infty})$$

$$\geq \gamma \|\nabla u\|_{q}^{q} + P_{h} \|u\|_{q}^{q} - C_{4} - C_{3}$$
(11)

with $C_4 = -\rho_s \int_{\Omega \setminus \Omega_m} U^{\mathrm{vdW}} \, d\mathbf{r}$, which implies $M_q := \inf_{u \in \mathcal{X}_q} I_q(u)$ is finite. Now we can find a minimizing sequence $\{w_k\}_{k=1}^{\infty} \subset \mathcal{X}_q$ such that $\lim_{k \to \infty} I_q(w_k) = M_q$. (11) implies that $\{w_k\}_{k=1}^{\infty}$ are uniformly bounded in \mathcal{X}_q . As a direct consequence, when q > 1, there exists some $u_q \in \mathcal{X}_q$ such

$$w_k \to u_q$$
 in $W^{1,q}(\Omega)$ and $w_k \to u_q$ in $L^q(\Omega)$ as $k \to \infty$;

or when q = 1, we apply [19, Theorem 5.2.3.4] to obtain some $u_1 \in \mathcal{X}_1$ such that $w_k \to u_1$ in $L^1(\Omega)$ as $k \to \infty$.

Finally, the lower semi-continuity of $I_{nn,q}(\cdot)$, cf. [18, Section 8.2.2] and [19, Theorem 5.2.1.1], Proposition 2.3 and the dominated convergence theorem imply that

$$M_q = I_q(u_q) \le \liminf_{k \to \infty} I_q(w_k),$$

and thus u_q is a global minimizer of $I_q(\cdot)$ with $I_q(u_q)$ finite.

When q > 1, the uniqueness of a global minimizer is a direct consequence of the strict convexity of $I_a(\cdot)$. Indeed, let $u_t = tu_0 + (1-t)u_1$ for $t \in [0,1]$ and $u_0, u_1 \in \mathcal{X}_q$ with $u_0 \neq u_1$. Then it follows from Proposition 2.2 that

$$\begin{split} I_q(u_t) = & I_{np,q}(u_t) + I_{p,q}(u_t, \psi_{u_t}) \\ < & t \left[I_{np,q}(u_0) + I_{p,q}(u_0, \psi_{u_t}) \right] + (1-t) \left[I_{np,q}(u_1) + I_{p,q}(u_1, \psi_{u_t}) \right] \\ \leq & t \left[I_{np,q}(u_0) + I_{p,q}(u_0, \psi_{u_0}) \right] + (1-t) \left[I_{np,q}(u_1) + I_{p,q}(u_1, \psi_{u_1}) \right] \\ = & t I_q(u_0) + (1-t)I_q(u_1), \end{split}$$

as $I_{np,q}$ is strictly convex when q > 1. \square

Remark 2.5. Lacking the strict convexity of $I_1(\cdot)$, in general, the minimizer of $I_1(\cdot)$ does not need to be unique.

2.4. Asymptotic behavior of $I_q(\cdot)$ as $q \to 1^+$

Let u_q minimize $I_q(\cdot)$. In this section, we will show that, when $\Sigma_i \in$ C^2 with $i \in \{0,1\}$, u_q converges to a minimizer of $I_1(\cdot)$ as $q \to 1^+$.

We will first prove two lemmas. To prepare for the necessary nota-

$$\Omega_{j,k} := \{ \mathbf{r} \in \Omega : \operatorname{dis}(\mathbf{r}, \Omega_j) < 1/k \} \quad \text{with } j \in \{m, s\}$$

$$\mathcal{Y}_k := \{ u \in \mathcal{X}_1 : u \equiv 1 \text{ in } \Omega_{m,k} \text{ and } u \equiv 0 \text{ in } \Omega_{s,k} \}, k \in \mathbb{N}.$$

Lemma 2.6. For every $f \in \mathcal{Y}_k$, there exists a sequence $\{f_n\}_{n=1}^{\infty} \subset C^{\infty}(\overline{\Omega})$ satisfying Constraints (2) and (3) such that

(i)
$$f_n \to f$$
 in $L^1(\Omega)$, and

(ii)
$$||Df_n||(\Omega) \rightarrow ||Df||(\Omega)$$
 as $n \rightarrow \infty$.

Proof. For any $\delta > 0$, let η_{δ} be the Friedrichs mollifying kernel. For any $n \in \mathbb{N}$, we choose $\epsilon_n > 0$ so small that

(a)
$$f_n:=\eta_{\epsilon_n}*f$$
 satisfies Constrain (3) and (b) $\|f_n-f\|_1\leq 1/n.$

(b)
$$||f_n - f||_1 \le 1/n$$

Constrain (2) is obviously fulfilled by f_n . Then, it holds $\lim_{n\to\infty} ||f_n-f||_1 =$

It remains to show (ii). [19, Theorem 5.2.1.1] implies that

$$||Df||(\Omega) \le \liminf_{n \to \infty} ||Df_n||(\Omega).$$

Extending f to be identically zero outside Ω , we can consider f as an element in $BV(\mathbb{R}^3)$. For any $\phi \in C_0^1(\Omega)$ with $\|\phi\|_{\infty} \leq 1$, we have

Y. Shao, E. Hawkins, K. Wang et al.

$$\begin{split} \int\limits_{\Omega} f_n \mathrm{div} \phi \, d\mathbf{r} &= \int\limits_{\Omega} \left(\eta_{\epsilon_n} * f \right) \mathrm{div} \phi \, d\mathbf{r} = \int\limits_{\Omega} f \, \mathrm{div} \left(\eta_{\epsilon_n} * \phi \right) \, d\mathbf{r} \\ &= \int\limits_{\mathbb{R}^3} f \, \mathrm{div} \left(\eta_{\epsilon_n} * \phi \right) \, d\mathbf{r} \leq \|Df\|(\mathbb{R}^3) = \|Df\|(\Omega). \end{split}$$

The inequality follows from the definition of BV-functions. Taking supremum over all such ϕ , we derive that

 $||Df_n||(\Omega) \le ||Df||(\Omega),$

which implies that

 $\limsup_{n\to\infty} \|Df_n\|(\Omega) \le \|Df\|(\Omega).$

This completes the proof. \Box

Lemma 2.7. For every $f \in \mathcal{X}_1$, we define $\{f_k\}_{k=1}^{\infty} \subset BV(\Omega)$ by

$$f_k(x) = \begin{cases} 1, & x \in \Omega_{m,k} \\ 0, & x \in \Omega_{s,k} \\ f(x), & elsewhere \end{cases}$$

If $\Sigma_i \in C^2$ with $i \in \{0, 1\}$, then

- (i) $f_k \to f$ in $L^1(\Omega)$ and
- (ii) $||Df_k||(\Omega) \rightarrow ||Df||(\Omega)$ as $k \rightarrow \infty$.

Proof. The proof for (i) is straightforward. So we will only show (ii). In the following proof, it is always assumed that $i \in \{0,1\}$. Since Σ_i are C^2 , there exists some $\mathfrak{a} > 0$ such that Σ_i has a tubular neighborhood $B_{\mathfrak{a}}(\Sigma_i)$ of width $\mathfrak{a} > 0$, cf. [23, Exercise 2.11] and [30, Remark 3.1]. Denote by v_i the outward pointing (into Ω_b) unit normal of Σ_i . Then the map defined by

$$\Lambda_i: \Sigma_i \times (-\mathfrak{a}, \mathfrak{a}) \to \mathbb{R}^3: (x, r) \mapsto x + r \nu_i(x)$$

is a C^1 -diffeomorphism; and $\Sigma_{i,r}:=\Lambda_i(\Sigma_i,r)$ is a C^1 -hypersurface, whose outward unit normal is denoted by $v_{i,r}$. In particular, $v_{i,0}=v_i$. By the inverse function theorem, there exist two maps $P_i\in C^1(B_\mathfrak{a}(\Sigma_i),\Sigma_i)$ and $d_i\in C^1(B_\mathfrak{a}(\Sigma_i),(-\mathfrak{a},\mathfrak{a}))$, where P_i is the nearest point projection onto Σ_i and d_i is the signed distance to Σ_i with $d_i(x)>0$ for $x\in B_\mathfrak{a}(\Sigma_i)\cap\Omega_b$. Note that d_i is indeed C^2 , see [37] for example. We can define two C^1 -vector fields $V_i:B_\mathfrak{a}(\Sigma_i)\to\mathbb{R}^3$ by

$$V_i(x) = v_{i,d_i(x)}(x).$$

For any $r \in (0, \mathfrak{a})$, put $U_{i,r} := B_r(\Sigma_i) \cap \Omega_b$. Due to the trace theorem of BV-functions, cf. [19, Theorem 5.3.1], we have

$$\int\limits_{U_{i,r}} f \operatorname{div} V_i \, d\mathbf{r} + \int\limits_{U_{i,r}} V_i \cdot d[Df] = \int\limits_{\Sigma_{i,r}} T_r f \, d\mathcal{H}^2 - \int\limits_{\Sigma_i} T_r f \, d\mathcal{H}^2$$

for all $f \in \mathcal{X}_1$ with \mathcal{H}^2 being the two-dimensional Hausdorff measure. Here $T_r f$ is the trace of $f|_{U_{i,r}}$ on $\partial U_{i,r}$; and [Df] is the vector-valued measure for the gradient of f.

Pushing $r \to 0^+$ above yields that

$$\lim_{r \to 0^{-}} \int_{\Sigma_{i,r}} T_r f \, d\mathcal{H}^2 = \int_{\Sigma_i} T_r f \, d\mathcal{H}^2. \tag{12}$$

[19, Theorem 5.2.1.1] implies that

 $||Df||(\Omega) \le \liminf_{k \to \infty} ||Df_k||(\Omega).$

Observe that $\partial\Omega_{m,k}=\Sigma_{1,1/k}$ and $\partial\Omega_{s,k}\setminus\partial\Omega=\Sigma_{0,1/k}$ for sufficiently large k. Denote by \tilde{T}_rf the trace of $f|_{\Omega_b\setminus \left(U_{0,r}\cup U_{1,r}\right)}$ on $\partial\left[\Omega_b\setminus \left(U_{0,r}\cup U_{1,r}\right)\right]$. Direct computations show

$$-\sum_{i=1}^{2} \left(\int_{\Sigma_{i,1/k}} \left| T_{1/k} f - \tilde{T}_{1/k} f \right| d\mathcal{H}^2 \right)$$

$$\leq \sum_{i=1}^{2} \left[\int\limits_{\Sigma_{i,1/k}} (1 - T_{1/k} f) d\mathcal{H}^{2} - \int\limits_{\Sigma_{i}} (1 - T_{1/k} f) d\mathcal{H}^{2} - \|Df\| (U_{i,1/k}) \right]$$

From (12), we infer that

$$\lim_{k \to \infty} \left[\int_{\Sigma_{i,1/k}} (1 - T_{1/k} f) d\mathcal{H}^2 - \int_{\Sigma_i} (1 - T_{1/k} f) d\mathcal{H}^2 - ||Df|| (U_{i,1/k}) \right] = 0.$$

This implies that

 $\limsup_{k \to \infty} \|Df_k\|(\Omega) \le \|Df\|(\Omega).$

This completes the proof. \Box

Theorem 2.8. Assume that $\Sigma_i \in C^2$ with $i \in \{0, 1\}$. As $q \to 1^+$, u_q converges to a minimizer u of $I_1(\cdot)$ in $L^p(\Omega)$ for any $1 \le p < \infty$. Moreover,

$$\lim_{q\to 1^+}I_q(u_q)=I_1(u).$$

Proof. Fix $v \in W^{1,q}(\Omega)$ satisfying Constraints (2) and (3). Then

$$\begin{split} I_q(v) &\leq \gamma \int\limits_{\Omega} |\nabla v|^q \, d\mathbf{r} + P_h \mathrm{Vol}(\Omega \setminus \Omega_m) + \int\limits_{\Omega_s} \rho_s U^{\mathrm{vdW}} \, d\mathbf{r} + C_0 \|\rho_m\|_{\infty} \mathrm{Vol}(\Omega_m) \\ &\leq C_5, \end{split}$$

where C_0 is the constant in Proposition 2.2 and C_5 is independent of q. This yields that

$$C_{5} \ge I_{q}(u_{q}) \ge \gamma \int_{\Omega} |\nabla u_{q}|^{q} d\mathbf{r} + P_{h} ||u||_{q}^{q} - C_{3} - C_{4}$$

$$\ge \left[\gamma ||\nabla u_{q}||_{1}^{q} + P_{h} ||u||_{1}^{q} \right] (\text{Vol}(\Omega))^{1-q} - C_{3} - C_{4}, \tag{13}$$

where C_3 and C_4 are the constants in the proof of Theorem 2.4. We thus infer from (13) that

$$||u_q||_{W^{1,1}} \le C_6$$

for some C_6 independent of q. [19, Theorem 5.2.3.4] implies that, given any sequence $q_n \to 1^+$, there exists a subsequence of $\{u_{q_n}\}_{n=1}^\infty$, not relabeled, converging to some $u \in \mathcal{X}_1$ in $L^1(\Omega)$. The Riesz-Thorin interpolation theorem then implies that $u_{q_n} \to u$ in $L^p(\Omega)$ for all $p \in [1, \infty)$ as $n \to \infty$. Note that

$$\int\limits_{\Omega} |\nabla u_q|^q d\mathbf{r} \ge \|\nabla u_q\|_1^q (\operatorname{Vol}(\Omega))^{1-q}.$$

Then it follows from [19, Theorem 5.2.1.1] and Proposition 2.3 that

$$I_1(u) \leq \liminf_{n \to \infty} I_{q_n}(u_{q_n}).$$

On the other hand, we define

$$w_k(x) = \begin{cases} 1, & x \in \Omega_{m,k} \\ 0, & x \in \Omega_{s,k} \\ u(x), & \text{elsewhere} \end{cases}$$

We will show that

$$\limsup I_{q_n}(u_{q_n}) \le I_1(w_k). \tag{14}$$

Lemma 2.6 implies that we can find a sequence $\{w_{k,i}\}_{i=1}^{\infty}$ such that $w_{k,i} \in C^{\infty}(\overline{\Omega}) \cap \mathcal{X}_q$ for all q and

$$w_{k,i} \to w_k$$
 in $L^1(\Omega)$ and $||Dw_{k,i}||(\Omega) \to ||Dw_k||(\Omega)$ as $i \to \infty$.

Since u_a minimizes $I_a(\cdot)$ in \mathcal{X}_a , we have

$$I_{a_{-}}(u_{a_{-}}) \leq I_{a_{-}}(w_{k,i}).$$

Pushing $n \to \infty$, the dominated convergence theorem implies that

$$\limsup I_{q_n}(u_{q_n}) \leq I_1(w_{k,i}).$$

Then Lemma 2.6 and Proposition 2.3 immediately yield (14). Now Lemma 2.7 and Proposition 2.3 imply that

$$\limsup_{n\to\infty} I_{q_n}(u_{q_n}) \le I_1(u). \quad \square$$

2.5. Variations and surface models

To prepare the theoretic basis for the numerical simulations, we will derive the first variation of the energy functional in the case $q \in (1,2]$. Because of the presence of the constrained admissible space, the resulted surface model is expected to be different from previous unconstrained smooth surface models. For simplicity, we will confine our attention to the minimization problem of the nonpolar energy which includes the surface energy term. By doing so, modeling uncertainties can be minimized by considering a relatively isolated situation in which electrostatic interactions between the solvent and solute are negligible. This is because different types of energies may contribute to uncertainties for the model comparision.

Because of Constrain (3), the nonpolar energy can be reduced to

$$I_{np,q}(u) = \tilde{I}_{np,q}(u) + M_0 \tag{15}$$

where $M_0 = P_h \text{Vol}(\Omega_m) + \rho_s \int_{\Omega_s} U^{\text{vdW}} d\mathbf{r}$ is independent of u and

$$\tilde{I}_{np,q}(u) = \int_{\Omega_h} \left[\gamma |\nabla u|^q + P_h u + \rho_s (1 - u) U^{\text{vdW}} \right] d\mathbf{r}$$
(16)

is the nonpolar energy contained in Ω_b .

Proposition 2.9. (16) has a unique global minimizer u_q in the admissible space

$$\mathcal{X}_a = \{u \in W^{1,q}(\Omega_b) : u = i \text{ on } \Sigma_i \text{ with } i = 0, 1 \text{ and } 0 \le u \text{ a.e. in } \Omega\}.$$

Moreover, $u_q \in \mathcal{X}_q$. Here it is understood that a function $v \in \mathcal{X}_q$ is automatically extended to be one in \mathcal{X}_q by

$$v(\mathbf{r}) = \begin{cases} 1 & \text{when } \mathbf{r} \in \Omega_m \\ v(\mathbf{r}) & \text{when } \mathbf{r} \in \Omega_b \\ 0 & \text{when } \mathbf{r} \in \Omega_s. \end{cases}$$

Proof. The existence and uniqueness of a global minimizer in \mathcal{X}_q follows from the strict convexity of $\tilde{I}_{np,q}(\cdot)$ and the direct method of Calculus of Variation. If $\mathcal{L}^3(\{u_q>1\})\neq 0$, we put

$$\bar{u}_q(\mathbf{r}) = \begin{cases} 1 & \text{if } u_q(\mathbf{r}) > 1; \\ u_q(\mathbf{r}) & \text{otherwise.} \end{cases}$$

[16, Proposition 20.2] again implies that $\bar{u}_q \in \mathcal{X}_q$ and a direct computation shows that

$$\tilde{I}_{np,q}(\bar{u}_q) < \tilde{I}_{np,q}(u_q).$$

A contradiction. Therefore, $u_q \in \mathcal{X}_q$. \square

Remarks 2.10.

- (i) The reason to enlarge the admissible space \mathcal{X}_q to \mathcal{X}_q is due to the following consideration. The first variation of (16) yields an obstacle problem of q-Laplacian equation. To study the variational formula, in the following, we will use the porosity of the free boundary of q-Laplacian with one-sided obstacle [25], which corresponds to the one-sided bound $0 \le u$ in the definition of \mathcal{X}_q . Such a result, nevertheless, is unknown for the two-sided bound $0 \le u \le 1$.
- (ii) Following the proof of Theorem 2.8, one can show that, considering u_q as an element in X_q, u_q → u in L¹(Ω) for some minimizer u of I_{np,1}(·) in X₁. Moreover,

$$\lim_{q \to 1^+} I_{np,q}(u_q) = I_{np,1}(u).$$

Pick any $\phi \in \mathcal{X}_a$ and let

$$\gamma(\tau) = (1-\tau)u_q + \tau \phi = u_q + \tau (\phi - u_q), \quad \tau \in [0,1].$$

Since \mathcal{X}_q is convex, we conclude that $\gamma(\tau)\in\mathcal{X}_q.$ Set $L(\tau)=I_{np,q}(\gamma(\tau)).$ Then

$$\begin{split} 0 \leq & L'(0) = \lim_{\tau \to 0^+} \frac{L(\tau) - L(0)}{\tau} \\ & = \int_{\Omega_h} \left[\gamma q |\nabla u_q|^{q-2} \nabla u_q \cdot \nabla (\phi - u_q) + (P_h - \rho_s U^{\text{vdW}}) (\phi - u_q) \right] \, d\mathbf{r}. \end{split}$$

Let
$$a: \mathcal{X}_a \times W_0^{1,q}(\Omega_b) \to \mathbb{R}$$
 be defined by

$$a(u,v) = \int_{\Omega_h} \left[\gamma q |\nabla u|^{q-2} \nabla u \cdot \nabla v + (P_h - \rho_s U^{\text{vdW}}) v \right] d\mathbf{r}.$$

We will show that there is a unique solution to the following variational inequality in \mathcal{X}_a

$$a(u, \phi - u) \ge 0$$
 for all $\phi \in \mathcal{X}_a$. (17)

A crucial step of the proof is the following estimate.

Lemma 2.11. There exist two positive constants c and C such that

$$\begin{split} c(\|u\|_{W^{1,q}} + \|v\|_{W^{1,q}})^{q-2}\|u-v\|_{W^{1,q}}^2 &\leq a(u,u-v) - a(v,u-v) \leq C\|u-v\|_{W^{1,q}}^q \\ &\text{for all } u,v \in \mathcal{Y}_q, \text{ where } \mathcal{Y}_q &:= \{w \in W^{1,q}(\Omega_b): w=i \text{ on } \Sigma_i \text{ with } i=0,1\}. \end{split}$$

Proof. Due to [41], it holds for all $\xi, \zeta \in \mathbb{R}^3$ and $1 < q \le 2$ that

$$\left| |\xi|^{q-2} \xi - |\zeta|^{q-2} \zeta \right| \le \tilde{C} |\xi - \zeta|^{q-1}$$
 (18)

and

$$\frac{|\xi - \zeta|^2}{(|\xi| + |\zeta|)^{2-q}} \le \tilde{c}(|\xi|^{q-2}\xi - |\zeta|^{q-2}\zeta) \cdot (\xi - \zeta). \tag{19}$$

The inequality $a(u,u-v)-a(v,u-v)\leq C\|u-v\|_{W^{1,q}}^q$ is immediate from (18). It follows from (19) that

$$a(u, u - v) - a(v, u - v) = \gamma q \int_{\Omega_b} \left(|\nabla u|^{q-2} \nabla u - |\nabla v|^{q-2} \nabla v \right) \cdot \nabla (u - v) d\mathbf{r}$$

$$\geq \gamma q \int_{\Omega_b} |\nabla (u - v)|^2 (|\nabla u| + |\nabla v|)^{q-2} d\mathbf{r}$$

$$\geq \gamma q ||\nabla (u - v)||_q^2 |||\nabla u| + |\nabla v|||_q^{q-2}$$
(20)

$$\geq c(\|u\|_{W^{1,q}} + \|v\|_{W^{1,q}})^{q-2} \|\nabla(u - v)\|_q^2. \tag{21}$$

In the above, (20) follows from the reverse Hölder inequality and (21) is a consequence of the Minkowski and Poincaré's inequalities. \square

Proposition 2.12. There is a unique solution to the variational inequality (17) in \mathcal{X}_a .

Proof. We already know that u_q is a solution to (17). It remains to show the uniqueness part. Assume to the contrary that (17) has two solutions $u, v \in \mathcal{X}_a$. (17) states that

$$0 \le a(u, v - u) + a(v, u - v).$$

On the other hand, the above lemma implies that

$$0 \ge a(u, u - v) - a(v, u - v) \ge c(\|u\|_{W^{1,q}} + \|v\|_{W^{1,q}})^{q-2} \|u - v\|_{W^{1,q}}^2,$$
 which yields $\|u - v\|_{W^{1,q}} = 0$ and thus $u = v$ a.e. in Ω_b . \square

We decompose Ω_b into

$$\Omega_b = \Omega_b^+ \sqcup \Omega_b^0$$
, where $\Omega_b^+ = \{ \mathbf{r} \in \Omega_b : u_a(\mathbf{r}) > 0 \}$.

Proposition 2.13. $u \in \mathcal{X}_q$ solves (17) iff u solves

$$\begin{cases} \Delta_q u = \frac{P_h - \rho_s U^{\text{vdW}}}{\gamma q} H(u) & \text{in } \Omega_b; \\ u = i & \text{on } \Sigma_i \end{cases}$$
 (22)

in \mathcal{Y}_a , where $\Delta_a u = \operatorname{div}(|\nabla u|^{q-2} \nabla u)$ is the q-Laplacian operator and

$$H(t) = \begin{cases} 1, & t > 0 \\ 0, & t \le 0. \end{cases}$$

Proof. (\Longrightarrow): In Proposition 2.12, we have shown that u_q is the unique solution to (17). It follows from [10, Theorem 1] that $u_q \in C(\Omega_b)$. Then, it is a well-known result that u_q solves

$$q\gamma \Delta_a u = P_h - \rho_s U^{\text{vdW}}$$

in Ω_h^+ , cf. [18, Section 8.4.2]. [25, Lemma 1.1] shows that

$$q\gamma \Delta_q u = (P_h - \rho_s U^{\text{vdW}}) \chi_{\Omega_b^+} - \mu \quad \text{in } \Omega_b$$

for some nonnegative Radon measure μ supported in $\partial \Omega_b^+$. Meanwhile, [25, Theorem 1.3] implies that $\mathcal{L}^3(\partial \Omega_b^+) = 0$. In this case, it is known that u_a solves (22). See also [39, Theorem 1.3] for a related problem.

 $(\stackrel{\cdot}{\rightleftharpoons})$: We already know that u_q is a solution to (22). If u and v solve (22) in \mathcal{Y}_a , then

$$\gamma q \int_{\Omega_b} \left[|\nabla u|^{q-2} \nabla u - |\nabla v|^{q-2} \nabla v \right] \cdot \nabla (u-v) \, d\mathbf{r}$$

$$+ \int_{\Omega_b} \left(P_h - \rho_s U^{\text{vdW}} \right) \left[H(u)(u-v) + H(v)(v-u) \right] \, d\mathbf{r} = 0.$$

Direct computations show $H(u)(u-v)+H(v)(v-u)\geq 0.$ It follows from Lemma 2.11 that

$$\begin{split} 0 = & \gamma q \int\limits_{\Omega_b} \left(|\nabla u|^{q-2} \nabla u - |\nabla v|^{q-2} \nabla v \right) \cdot \nabla (u-v) \, d\mathbf{r} \\ + \int\limits_{\Omega_b} \left(P_h - \rho_s U^{\text{vdW}} \right) \left[H(u)(u-v) + H(v)(v-u) \right] \, d\mathbf{r} \\ \ge & c (\|u\|_{W^{1,q}} + \|v\|_{W^{1,q}})^{q-2} \|u-v\|_{W^{1,q}}^2. \end{split}$$

This implies that u=v a.e. in Ω_b . Therefore, u_q is the unique solution to (22) in \mathcal{Y}_q . \square

3. Computational schemes and simulation results

3.1. Numerical implementation

The nonpolar free energy functional of solvation for biomolecules at equilibrium is given by

$$I_{np,q} = \int_{\Omega} \left[\gamma |\nabla u(\mathbf{r})|^q + P_h u(\mathbf{r}) + \rho_s (1 - u(\mathbf{r})) U^{\text{vdW}}(\mathbf{r}) \right] d\mathbf{r}.$$
 (23)

To obtain the optimal function u, we rewrite the equation (22) into

$$\begin{cases} -\gamma q \Delta_q u + (P_h - \rho_s U^{\text{vdW}}) H(u) = 0 & \text{in} \quad \Omega_b; \\ u = i & \text{on} \quad \Sigma_i, \end{cases}$$
 (24)

where $\Delta_q u$ is the q-Laplacian operator. γ is a parameter constant. The solution u of (24) is regarded as our "diffuse solvent-solute boundary" to calculate the solvation free energy based on (23). Actually, the solution of the above PDE can be attained via a parabolic PDE as discussed in earlier work [3,7].

$$\frac{\partial u}{\partial t} = |\nabla u|^{2-q} \left[\operatorname{div} \left(\gamma q \frac{\nabla u}{|\nabla u|^{2-q}} \right) + V \right], \tag{25}$$

where the generalized "potential" V is defined as

$$V = (-P_h + \rho_s U^{\text{vdW}})H(u). \tag{26}$$

Finally, in (25), as $t \to \infty$, the initial profile of u evolves into a steady state solution, which solves the original (24).

Numerically, the equation (25) can be rewritten in the form [3].

$$\begin{split} \frac{\partial u}{\partial t} &= \gamma q \frac{(u_x^2 + u_y^2 + (q-1)u_z^2)u_{zz} + (u_x^2 + (q-1)u_y^2 + u_z^2)u_{yy} + ((q-1)u_x^2 + u_y^2 + u_z^2)u_{xx}}{u_x^2 + u_y^2 + u_z^2} \\ &- \gamma (2-q)q \frac{2u_xu_yu_{xy} + 2u_xu_zu_{xz} + 2u_zu_yu_{yz}}{u_x^2 + u_y^2 + u_z^2} + (\sqrt{u_x^2 + u_y^2 + u_z^2})^{2-q}V. \end{split}$$

The explicit scheme is applied to the time-dependent derivative. Finite difference schemes are used for the first and second order derivatives with respect to space coordinates as we did previously [7]. To implement the domain decomposition in (3), u is fixed to be one in the pure solute area Ω_m enclosed by van der Waals surface (vdW). u is fixed to be zero in the pure solvent domain Ω_s outside solvent accessible surface (SAS). In practice, a few smoothing steps are applied to make Σ_0 and Σ_1 to be C^2 . In addition, a simple relaxing scheme is applied to the solution process of interface equation (25) to guarantee its convergence as follows:

$$u = \alpha u_{new} + (1 - \alpha)u_{old}. \tag{28}$$

 u_{new} and u_{old} denote the new and old u values from the current and previous time steps, respectively. We set $\alpha=0.5$ for the simulation here. Finally, a simple cutoff strategy is conducted to apply Constraint (2) and to avoid possible numerical errors:

$$u = \begin{cases} u(x) & u \in [0,1] \\ 0 & u < 0 \\ 1 & u > 1. \end{cases}$$
 (29)

The cutoff checkup is carried out every time step or several steps during the solution of equation (27). Finally, a very small number, such as 10^{-6} , is added to the denominator to avoid possible zeros in the denominator [7].

Regarding the parameterization, we adopt a previous simple strategy [8]. We fix the solvent density ρ_s to be 0.0334 1/ų [8,44], the solvent radius $\sigma_s=0.65$ Å, and the carbon atom radius $\sigma_c=1.87$ Å. Meanwhile, γ , P_h , ϵ_{hs} and ϵ_{cs} are considered as fitting parameters. Note that ϵ_{hs} and ϵ_{cs} are well depth parameters of the hydrogen and carbon, respectively. Eventually, an iterative procedure is designed as follows:

Table 1 Different optimized parameters and RMS errors from various q values.

q value	γ (kcal/(mol Å ²))	P_h (kcal/(mol Å ³))	ϵ_{cs} (kcal/mol)	RMS (kcal/mol)
1.5	0.0017	0.000	0.461	0.187
1.3	0.0072	0.000	0.412	0.280
1.1	0.032	0.019	0. 50	0.108
1.05	0.0493	0.013	0.492	0.108
1.01	0.0687	0.010	0.488	0.109
1.001	0.0740	0.009	0.486	0.109
1.00001	0.0746	0.009	0.486	0.109

Step 0: We choose an initial set of fitting parameters and a trial set of molecules with existing atomic coordinates, radii, and experimental data of solvation free energies.

Step 1: For the *j*-th molecule, (25) is solved to find the solution of u_j with current parameter values, $j=1,\cdots,N_m$. Here N_m represents the total number of molecules in the trial set.

Step 2: All non-negative parameters P_h , γ , and ϵ_{is} are determined and updated by a non-negative least squares algorithm via minimizing a target function

$$T = \min_{(p,\gamma,\epsilon_{is})} \sum_{j=1}^{N_m} \left(I_{np,q}^j - I_{np,q}^{j,\mathrm{exp}} \right)^2,$$

where $I_{np,q}^{j,exp}$ is known experimental data of solvation free energies for the i-th molecule.

Step 3: The iterative loop step 1 and step 2 continue until all fitting parameters converge within a pre-set tolerance.

3.2. Simulation results

In this subsection, for the purpose of numerical simulation and convergence demonstration, a set of 11 alkanes is chosen as a calibration set which includes linear, branched, and cyclic apolar compounds. Meanwhile, it serves as the trial set of molecules for the above parameterization process. In the present work, nonpolar solvation free energy is calculated by (23) containing terms related to surface area, volume, and Lennard-Jones (LJ) solvent-solute interactions. The repulsive and attractive parts of solvation free energy can be calculated separately in the present model. Specifically, first two terms of (23) count for the repulsive part of solvation free energy. This allows a detailed comparison of our variational model with different q values and with other computational methods [22].

3.2.1. Model validation

The parameter constant q in the surface energy term of (23) needs to be determined for model validation and solvation energy calculation and prediction. For an arbitrary q between 1 and 2, optimal fitting parameters can be found and then corresponding diffuse interface and solvation free energy will be computed. For example, for the set of 11 alkane compounds with q = 1.1, optimized fitting parameters are obtained: surface tension $\gamma = 0.032 \text{ kcal/(mol Å}^2)$, solvent pressure $P_h = 0.0186$ kcal/(mol Å³), LJ parameters $\epsilon_{cs} = 0.50$ kcal/mol, and ϵ_{hs} = 0.00 kcal/mol. The root mean square (RMS) error is obtained to be 0.108 kcal/mol. It turns out that different q values lead to different optimized parameter set. q is not close enough to 1 (greater than or equal to 1.3), the numerical result may become non-physical. For instance, one may obtain zero for the optimized solvent pressure P_h through the non-negative least squares algorithm. Zero pressure is non-physical regarding the solvation process. In contrast, when q is close enough to 1, it is evident that our model accurately catches subtle differences between linear, branched, and cyclic apolar compounds by reproducing the total solvation free energies of 11 alkanes. Different optimized parameters and RMS errors from various q values are shown in Table 1.

Note that, when $q \in (1,2]$, the solution u of the PDE system (24) can never be identically 1 or 0 in the transition region of Ω_b . For otherwise,

Table 2 Computed total solvation free energies of the trial set of 11 alkane compounds and their repulsive and attractive decomposition when q = 1.00001. $\gamma = 0.0746$ kcal/(mol Å²), $P_h = 0.0090$ kcal/(mol Å³) and $\epsilon_{cs} = 0.486$ kcal/mol, and $\epsilon_{hs} = 0.00$ kcal/mol

Compound	Rep. part	Att. part	Numerical	Experimental [6		
	(kcal/mol)					
methane	4.21	-2.21	2.00	2.00		
ethane	5.90	-3.95	1.95	1.83		
propane	9.00	-6.89	2.12	1.96		
butane	7.45	-5.42	2.03	2.08		
pentane	10.58	-8.28	2.30	2.33		
hexane	12.13	-9.75	2.38	2.49		
isobutane	8.90	-6.64	2.26	2.52		
2-methylbutane	10.20	-7.80	2.40	2.38		
neopentane	10.21	-7.61	2.60	2.50		
cyclopentane	9.21	-8.04	1.17	1.20		
cyclohexane	10.45	-9.08	1.37	1.23		
RMS of calibration set			0.109			

Table 3 Computed total solvation free energies of 11 alkene compounds and their repulsive and attractive decomposition when q=1.00001. The fitting parameters are taken from the above trial set: $\gamma=0.0746$ kcal/(mol Ų), $P_h=0.0090$ kcal/(mol ų), $\epsilon_{rs}=0.496$ kcal/mol, and $\epsilon_{hs}=0.00$ kcal/mol.

Compound	Rep. part	Att. part	Numerical	Experimental [38]		
	(kcal/mol)					
3-methyl-1-butene	10.15	-8.32	1.84	1.82		
1-butene	8.68	-7.04	1.64	1.38		
ethene	5.51	-4.12	1.49	1.27		
1-heptene	13.42	-11.58	1.84	1.66		
1-hexene	11.83	-10.05	1.78	1.68		
1-nonene	16.64	-14.59	1.95	2.06		
2-methyl-2-butene	10.08	-8.33	1.74	1.31		
1-octene	14.99	-13.01	1.98	2.17		
1-pentene	10.22	-8.58	1.65	1.66		
1-propene	7.12	-5.59	1.53	1.27		
trans-2-heptene	13.45	-11.62	1.83	1.66		
RMS of prediction set			0.21			

it will violate the fact that $u \in W^{1,p}(\Omega)$. Some numerical evidence can be found in Figure (2) in which a smooth transition region can be easily observed in-between two atoms even for a simple two-atom system.

Moreover, as $q \to 1^+$, the corresponding solvation energies converge as described in Remark 2.10 (ii) and proved in Theorem 2.8. Therefore, when q is very close to 1, the numerical results of solvation free energy calculated by the generalized constrained solvation model can be considered as counterpart results of the proposed constrained solvation model when q=1. Because of that, we choose q=1.00001 to validate our constrained solvation model. With the above set of 11 alkanes, new optimized fitting parameters are obtained for q=1.00001: $\gamma=0.0746$ kcal/(mol Ų), $P_h=0.0090$ kcal/(mol ų) and $\epsilon_{cs}=0.486$ kcal/mol, and $\epsilon_{hs}=0.00$ kcal/mol. It also reproduces the total solvation free energies of 11 alkanes very well (see Table 2). The root mean square (RMS) error is 0.109 kcal/mol.

Moreover, with q=1.00001 we conduct a predictive study for a set of previously-used 11 alkene compounds [8,9,38]. The above-obtained optimized parameters of q=1.00001 are utilized assuming the same solvent behavior. Solvation free energies of 11 alkene compounds are shown in Table 3, as well as their repulsive and attractive decomposition. Our numerical predictions match the experimental data, and their correlation is illustrated in Fig. 3 together with the comparisons for 11 alkanes. The RMS error of 11 alkenes is 0.21 kcal/mol.

3.2.2. Minimized energy converges when $q \rightarrow 1^+$

In view of Theorem 2.8, as $q \to 1^+$, the corresponding solvation energies converge to that with q=1. Therefore, it is meaningful to verify the convergence numerically when $q \to 1^+$. We let the value of q go to 1 by

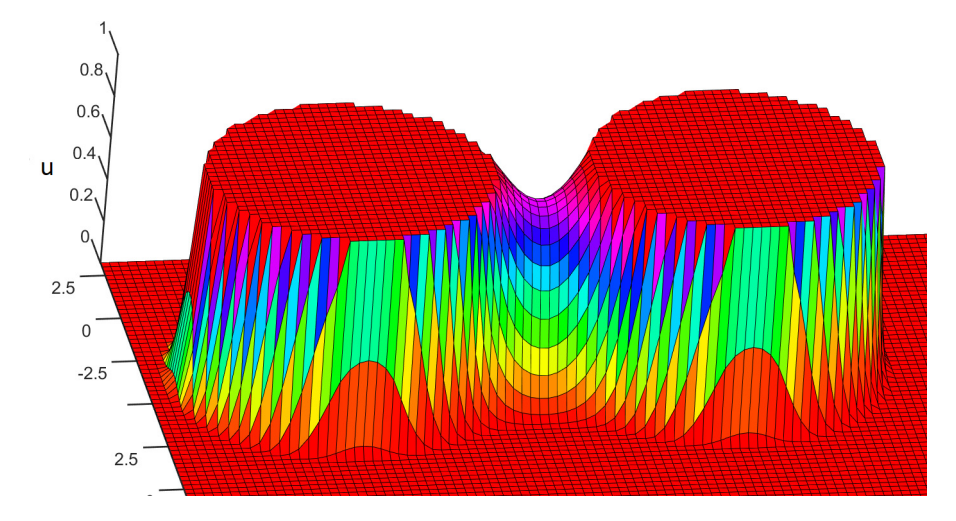


Fig. 2. A cross-section view of u profile for a two-ball system (1.4,0,0) and (-3,0,0) with radus 2 Å. Here those fitting parameters are obtained for q=1.00001: $\gamma=0.0746$ kcal/(mol Å²), $P_h=0.0090$ kcal/(mol Å³) and $\varepsilon_{cs}=0.486$ kcal/mol. It is shown that a smooth transition region can be observed around and in-between two atoms even for a simple two-atom system. Note that when $q\in(1,2]$, the solution u of the PDE system of (24) can never be identically 1 or 0 in the transition region Ω_b .

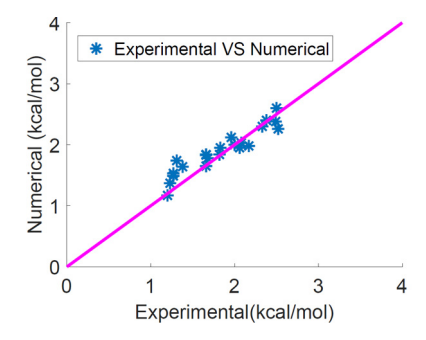


Fig. 3. Comparison of computed and experimental data of solvation free energies of 11 alkanes and 11 alkenes when q = 1.

Table 4 Convergence of total solvation free energies of eleven alkene molecules when $q \longrightarrow 1^+$ e.g. $q=1.01,\ 1.001,\ 1.0001,\ 1.00001,\ 1.000001.$ The fitting parameters are fixed as $\gamma=0.0746$ kcal/(mol Ų), $P_h=0.0090$ kcal/(mol ų), $\epsilon_{cs}=0.496$ kcal/mol, and $\epsilon_{hs}=0.00$ kcal/mol.

Compound	1.01	1.001	1.0001	1.00001	1.000001			
	(kcal/mo	(kcal/mol)						
3-methyl-1-butene	2.567	1.908	1.844	1.837	1.837			
1-butene	2.268	1.701	1.647	1.641	1.641			
ethene	1.888	1.524	1.489	1.485	1.485			
1-heptene	2.797	1.930	1.846	1.837	1.837			
1-hexene	2.625	1.857	1.784	1.776	1.775			
1-nonene	3.126	2.060	1.957	1.946	1.946			
2-methyl-2-butene	2.468	1.751	1.744	1.745	1.745			
1-octene	3.049	2.083	1.990	1.980	1.980			
1-pentene	2.381	1.716	1.653	1.646	1.645			
1-propene	2.043	1.575	1.530	1.525	1.525			
trans-2-heptene	2.789	1.918	1.835	1.826	1.826			

choosing a finite sequence of q (q = 1.01, 1.001, 1.0001, 1.00001, 1.00001, 1.00001) while fixing other model settings and parameters. Using the above set of alkene compounds, we compute the total solvation free energy for each alkene as well as its repulsive and attractive energy decomposition. It turns out that all of three energy quantities converge for all eleven alkene compounds. Table 4 demonstrates the convergence of total solvation free energy for the eleven molecules.

3.2.3. Comparison with previous GFBSS

If q = 1, the numerical implementation of proposed constrained solvation model turns out to be the same as the previous unconstrained nonpolar GFBSS model [8] with numerical constraints except for the following: in the presence of a two-sided obstacle for the characteristic function, the derived interface equation (24) is slightly different from previous unconstrained one [7,8]. Specifically, with constrained admissible space, there is a H(x) function in the current interface equation. It is unclear yet whether H(x) plays an important role on the surface generation and then solvation free energy calculation. To check it, by using the same parameter set as above we compare the computational results of 11 alkanes and 11 alkenes between the generalized constrained model (with H(x) and q = 0.00001) and the unconstrained GFBSS model (without H(x) and q = 1). It is shown that the numerical difference between them is negligible. See Table 5. It implies that the newly proposed constrained solvation model and the previous unconstrained one are equivalent to each other in terms of the solvation free energy calculation and prediction.

4. Conclusion

Variational based solvation models of biomolecules with smooth interface have drawn attentions in the past decade, since they have been developed as an efficient and reliable representation of solute-solvent interfaces in the framework of implicit solvent models. This work has provided solid mathematical supports for a previous promising geometric flow based computational model (GFBSS) of solvation and its involved computational treatment. For this purpose, we introduce a family of constrained variational solvation model with a parameter $q \in [1,2]$. In particular, when q=1, the newly proposed model is equivalent to the previous GFBSS model with two physical constraints: (1) a novel experimental based domain decomposition, and (2) a two-sided obstacle for the characteristic function describing the optimal diffuse solute-solvent boundary. These constraints correspond to two previously adopted computational schemes in the numerical implementation of the GFBSS model.

The properties of the constrained solvation energy functional have been studied. It is shown that the resulting model is mathematically well-posed. Particularly, the existence of a global minimizer of the proposed functionals has been proved; and the uniqueness is established when $1 < q \le 2$. Moreover, we obtain the convergence of the solvation energies and its unique minimizer u as $q \to 1^+$ to the case q = 1. The convergence of the energies to the unconstrained model has also been verified numerically when $q \to 1^+$.

Table 5 Comparisons of nonpolar solvation energies between previous unconstrained GFBSS (without H(x)) model and current constrained smooth interface solvation model (with H(x)) in which repulsive, attractive parts and total energies are compared with the above parameter set: $\gamma = 0.0746$ kcal/(mol Å²), $P_h = 0.0090$ kcal/(mol Å³), $\epsilon_{cs} = 0.496$ kcal/mol, and $\epsilon_{hs} = 0.00$ kcal/mol.

Compound	Rep. part (kcal/mol)		Att. part (kcal/mol)		Total (kcal/mol)	
	H(x)	W/O H(x)	H(x)	W/O H(x)	H(x)	W/O H(x)
methane	4.21	4.21	-2.21	-2.21	2.00	2.00
ethane	5.90	5.90	-3.95	-3.95	1.95	1.95
butane	9.00	9.00	-6.89	-6.89	2.12	2.12
propane	7.45	7.45	-5.42	-5.41	2.03	2.03
pentane	10.58	10.58	-8.28	-8.27	2.30	2.30
hexane	12.13	12.13	-9.75	-9.75	2.38	2.38
isobutane	8.90	8.90	-6.64	-6.64	2.26	2.26
2-methylbutane	10.20	10.20	-7.80	-7.80	2.40	2.40
neopentane	10.21	10.21	-7.61	-7.61	2.60	2.60
cyclopentane	9.21	9.21	-8.04	-8.04	1.17	1.17
cyclohexane	10.45	10.45	-9.08	-9.08	1.37	1.37
3-methyl-1- butene	10.15	10.15	-8.32	-8.32	1.84	1.83
1-butene	8.68	8.68	-7.04	-7.04	1.64	1.64
ethene	5.51	5.51	-4.12	-4.03	1.49	1.48
1-heptene	13.42	13.42	-11.58	-11.58	1.84	1.83
1-hexene	11.83	11.83	-10.05	-10.06	1.78	1.77
1-nonene	16.64	16.54	-14.59	-14.60	1.95	1.94
2-methyl-2-butene	10.08	10.08	-8.33	-8.33	1.74	1.74
1-octene	14.99	14.99	-13.01	-13.01	1.98	1.98
1-pentene	10.22	10.22	-8.58	-8.58	1.65	1.64
1-propene	7.12	7.12	-5.59	-5.60	1.53	1.52
trans-2-heptene	13.45	13.45	-11.62	-11.63	1.83	1.82

Further, when $q \in (1,2]$, the variation analysis of the constrained solvation free energy functional results in a variational inequality whose solution is proved to be equivalent to the solution of a PDE based interface equation. Although the new interface equation differs slightly from the previous interface equation, its numerical difference from the previous unconstrained model turns out to be negligible when $q \to 1^+$. This implies that the newly proposed constrained solvation model with q = 1 and the previous unconstrained one are equivalent to each other in terms of the solvation free energy calculation and prediction. Our model validation, its numerical implementation, and solvation energy convergence have been demonstrated using several common biomolecular modeling tasks, including one challenging set of 11 alkane molecules and one set of 11 alkene molecules. Note that, numerically, this work is limited to the study of nonpolar biomolecules to minimize modeling uncertainty by considering a relatively isolated situation in which electrostatic interactions between the solvent and solute are negligible.

For the future work, various analytic properties of the case q=1 will be intensively explored in a subsequent manuscript. Numerically, variational analysis and simulation studies will be extended to polar molecules and various applications. In addition, more advanced and efficient computation and parameterization strategies will be examined for the proposed models such as parallel computing.

Acknowledgements

This work is supported in part by National Science Foundation (NSF) grant No. DMS-1818748 (Z. Chen).

References

- [1] Ariel Abrashkin, David Andelman, Henri Orland, Dipolar Poisson-Boltzmann equation: ions and dipoles close to charge interfaces, Phys. Rev. Lett. 99 (7) (2007) 077801.
- [2] N.A. Baker, Improving implicit solvent simulations: a Poisson-centric view, Curr. Opin. Struct. Biol. 15 (2) (2005) 137–143.
- [3] P.W. Bates, Z. Chen, Y.H. Sun, G.W. Wei, S. Zhao, Geometric and potential driving formation and evolution of biomolecular surfaces. J. Math. Biol. 59 (2009) 193–231.
- [4] Klemen Bohinc, Guilherme Volpe Bossa, Sylvio May, Incorporation of ion and solvent structure into mean-field modeling of the electric double layer, Adv. Colloid Interface Sci. 249 (2017) 220–233.

- [5] A.H. Boschitsch, M.O. Fenley, Hybrid boundary element and finite difference method for solving the nonlinear Poisson-Boltzmann equation, J. Comput. Chem. 25 (7) (2004) 935–955.
- [6] S. Cabani, P. Gianni, V. Mollica, L. Lepori, Group contributions to the thermodynamic properties of non-ionic organic solutes in dilute aqueous solution, J. Solution Chem. 10 (8) (1981) 563–595.
- [7] Z. Chen, N.A. Baker, G.W. Wei, Differential geometry based solvation models I: Eulerian formulation, J. Comput. Phys. 229 (2010) 8231–8258.
- [8] Zhan Chen, Minimization and Eulerian formulation of differential geormetry based nonpolar multiscale solvation models, Comput. Math. Biophys. 4 (1) (2016).
- [9] Zhan Chen, Shan Zhao, Jaehun Chun, Dennis G. Thomas, Nathan A. Baker, Peter W. Bates, G.W. Wei, Variational approach for nonpolar solvation analysis, J. Chem. Phys. 137 (8) (2012) 084101.
- [10] Hi Jun Choe, John L. Lewis, On the obstacle problem for quasilinear elliptic equations of p Laplacian type, SIAM J. Math. Anal. 22 (3) (1991) 623–638.
- [11] Marco Cicalese, Cristina Trombetti, Asymptotic behaviour of solutions to p-Laplacian equation, Asymptot. Anal. 35 (1) (2003) 27–40.
- [12] Shibin Dai, Bo Li, Jianfeng Lu, Convergence of phase-field free energy and boundary force for molecular solvation, Arch. Ration. Mech. Anal. 227 (1) (2018) 105–147.
- [13] Michael D. Daily, Jaehun Chun, Alejandro Heredia-Langner, Guowei Wei, Nathan A. Baker, Origin of parameter degeneracy and molecular shape relationships in geometric-flow calculations of solvation free energies, J. Chem. Phys. 139 (20) (2013) 204108.
- [14] M.E. Davis, J.A. McCammon, Electrostatics in biomolecular structure and dynamics, Chem. Rev. 94 (1990) 509–521.
- [15] Françoise Demengel, On some nonlinear partial differential equations involving the "1"-Laplacian and critical Sobolev exponent, ESAIM Control Optim. Calc. Var. 4 (1999) 667–686.
- [16] Emmanuele DiBenedetto, Real Analysis, Birkhäuser Advanced Texts: Basler Lehrbücher (Birkhäuser Advanced Texts: Basel Textbooks), Birkhäuser Boston, Inc., Boston, MA, 2002.
- [17] J. Dzubiella, J.M.J. Swanson, J.A. McCammon, Coupling hydrophobicity, dispersion, and electrostatics in continuum solvent models. Phys. Rev. Lett. 96 (2006) 087802.
- [18] Lawrence C. Evans, Partial Differential Equations, second edition, Graduate Studies in Mathematics, vol. 19, American Mathematical Society, Providence, RI, 2010.
- [19] Lawrence C. Evans, Ronald F. Gariepy, Measure Theory and Fine Properties of Functions, Studies in Advanced Mathematics, CRC Press, Boca Raton, FL, 1992.
- [20] M. Feig, C.L. Brooks III, Recent advances in the development and application of implicit solvent models in biomolecule simulations, Curr. Opin. Struct. Biol. 14 (2004) 217–224
- [21] F. Fogolari, A. Brigo, H. Molinari, The Poisson-Boltzmann equation for biomolecular electrostatics: a tool for structural biology, J. Mol. Recognit. 15 (6) (2002) 377–392.
- [22] E. Gallicchio, M.M. Kubo, R.M. Levy, Enthalpy-entropy and cavity decomposition of alkane hydration free energies: numerical results and implications for theories of hydrophobic solvation, J. Phys. Chem. B 104 (26) (2000) 6271–6285.
- [23] David Gilbarg, Neil S. Trudinger, Elliptic Partial Differential Equations of Second Order, second edition, Grundlehren der Mathematischen Wissenschaften (Fundamental Principles of Mathematical Sciences), vol. 224, Springer-Verlag, Berlin, 1983.
- [24] P. Grochowski, Joanna Trylska, Continuum molecular electrostatics, salt effects and counterion binding. A review of the Poisson-Boltzmann theory and its modifications, Biopolymers 89 (2) (2007) 93–113.
- [25] L. Karp, T. Kilpeläinen, A. Petrosyan, H. Shahgholian, On the porosity of free boundaries in degenerate variational inequalities, J. Differ. Equ. 164 (1) (2000) 110–117.
- [26] Bernhard Kawohl, On a family of torsional creep problems, J. Reine Angew. Math. 410 (1990) 1–22.
- [27] P. Koehl, Electrostatics calculations: latest methodological advances, Curr. Opin. Struct. Biol. 16 (2) (2006) 142–151.
- [28] Patrice Koehl, Henri Orland, Marc Delarue, Beyond the Poisson-Boltzmann model: modeling biomolecule-water and water-water interactions, Phys. Rev. Lett. 102 (8) (2009) 087801.
- [29] G. Lamm, The Poisson-Boltzmann equation, in: K.B. Lipkowitz, R. Larter, T.R. Cundari (Eds.), Reviews in Computational Chemistry, John Wiley and Sons, Inc., Hoboken, N.J., 2003, pp. 147–366.
- [30] Jeremy LeCrone, Yuanzhen Shao, Gieri Simonett, The surface diffusion and the Willmore flow for uniformly regular hypersurfaces, Discrete Contin. Dyn. Syst., Ser. S 13 (12) (2020) 3503–3524.
- [31] R.M. Levy, L.Y. Zhang, E. Gallicchio, A.K. Felts, On the nonpolar hydration free energy of proteins: surface area and continuum solvent models for the solute-solvent interaction energy, J. Am. Chem. Soc. 125 (31) (2003) 9523–9530.
- [32] Bo Li, Xiaoliang Cheng, Zhengfang Zhang, Dielectric boundary force in molecular solvation with the Poisson-Boltzmann free energy: a shape derivative approach, SIAM J. Appl. Math. 71 (6) (2011) 2093–2111.
- [33] Bo Li, Yuan Liu, Diffused solute-solvent interface with Poisson-Boltzmann electrostatics: free-energy variation and sharp-interface limit, SIAM J. Appl. Math. 75 (5) (2015) 2072–2092.
- [34] A. Mercaldo, S. Segura de León, C. Trombetti, On the behaviour of the solutions to p-Laplacian equations as p goes to 1, Publ. Mat. 52 (2) (2008) 377–411.
- [35] A. Mercaldo, S. Segura de León, C. Trombetti, On the solutions to 1-Laplacian equation with L^1 data, J. Funct. Anal. 256 (8) (2009) 2387–2416.

- [36] Anna Mercaldo, Julio D. Rossi, Sergio Segura de León, Cristina Trombetti, Behaviour of p-Laplacian problems with Neumann boundary conditions when p goes to 1, Commun. Pure Appl. Anal. 12 (1) (2013) 253–267.
- [37] Jan Prüss, Gieri Simonett, On the manifold of closed hypersurfaces in ℝⁿ, Discrete Contin. Dyn. Syst. 33 (11–12) (2013) 5407–5428.
- [38] E.L. Ratkova, G.N. Chuev, V.P. Sergiievskyi, M.V. Fedorov, An accurate prediction of hydration free energies by combination of molecular integral equations theory with structural descriptors, J. Phys. Chem. B 114 (37) (2010) 12068–12079.
- [39] José Francisco Rodrigues, Stability remarks to the obstacle problem for *p*-Laplacian type equations, Calc. Var. Partial Differ. Equ. 23 (1) (2005) 51–65.
- [40] B. Roux, T. Simonson, Implicit solvent models, Biophys. Chem. 78 (1–2) (1999) 1–20.
- [41] Jacques Simon, Régularité de la solution d'une équation non linéaire dans \mathbb{R}^N , in: Journées d'Analyse Non Linéaire, Proc. Conf., Besançon, 1977, in: Lecture Notes in Math., vol. 665, Springer, Berlin, 1978, pp. 205–227.
- [42] Z.J. Tan, S.J. Chen, Electrostatic correlations and fluctuations for ion binding to a finite length polyelectrolyte, J. Chem. Phys. 122 (2005) 044903.
- [43] Dennis G. Thomas, Jaehun Chun, Zhan Chen, Guowei Wei, Nathan A. Baker, Parameterization of a geometric flow implicit solvation model, J. Comput. Chem. 34 (8) (2013) 687–695.

- [44] J.A. Wagoner, N.A. Baker, Assessing implicit models for nonpolar mean solvation forces: the importance of dispersion and volume terms, Proc. Natl. Acad. Sci. USA 103 (22) (2006) 8331–8336.
- [45] Bao Wang, G.W. Wei, Parameter optimization in differential geometry based solvation models, J. Chem. Phys. 143 (13) (2015) 134119.
- [46] A. Warshel, P.K. Sharma, M. Kato, W.W. Parson, Modeling electrostatic effects in proteins, Biochim. Biophys. Acta, Proteins Proteomics 1764 (11) (2006) 1647–1676.
- [47] Guo Wei Wei, Nathan A. Baker, Differential geometry-based solvation and electrolyte transport models for biomolecular modeling: a review, in: Many-Body Effects and Electrostatics in Biomolecules, Jenny Stanford Publishing, 2016, pp. 435–480.
- [48] Shan Zhao, Pseudo-time-coupled nonlinear models for biomolecular surface representation and solvation analysis, Int. J. Numer. Methods Biomed. Eng. 27 (12) (2011) 1964–1981.
- [49] Shan Zhao, Operator splitting adi schemes for pseudo-time coupled nonlinear solvation simulations, J. Comput. Phys. 257 (2014) 1000–1021.
- [50] Yanxiang Zhao, Yuen-Yick Kwan, Jianwei Che, Bo Li, J. Andrew McCammon, Phase-field approach to implicit solvation of biomolecules with Coulomb-field approximation, J. Chem. Phys. 139 (2) (2013) 024111.